LA-UR-02-7357

Approved for public release;
distribution is unlimited.

Title: ANALYTICAL SOLUTION ON THE TRANSIENT CORROSION/PRECIPITATION IN NON-ISOTHERMAL LBE FLOW LOOPS

Author(s): Jinsuo Zhang, 183022 - T-CNLS
Ning Li, 098012 - FWO-CMR

Submitted to: Corrosion

Los Alamos National Laboratory, an affirmative action/equal opportunity employer, is operated by the University of California for the U.S. Department of Energy under contract W-7405-ENG-36. By acceptance of this article, the publisher recognizes that the U.S. Government retains a nonexclusive, royalty-free license to publish or reproduce the published form of this contribution, or to allow others to do so, for U.S. Government purposes. Los Alamos National Laboratory requests that the publisher identify this article as work performed under the auspices of the U.S. Department of Energy. Los Alamos National Laboratory strongly supports academic freedom and a researcher's right to publish; as an institution, however, the Laboratory does not endorse the viewpoint of a publication or guarantee its technical correctness.

Form 836 (8/00)

LA-UR-02-7357

Approved for public release;
distribution is unlimited.

Title: ANALYTICAL SOLUTION ON THE TRANSIENT CORROSION/PRECIPITATION IN NON-ISOTHERMAL LBE FLOW LOOPS

Author(s): Jinsuo Zhang, 183022 - T-CNLS
Ning Li, 098012 - FWO-CMR

Submitted to: Corrosion

Los Alamos National Laboratory, an affirmative action/equal opportunity employer, is operated by the University of California for the U.S. Department of Energy under contract W-7405-ENG-36. By acceptance of this article, the publisher recognizes that the U.S. Government retains a nonexclusive, royalty-free license to publish or reproduce the published form of this contribution, or to allow others to do so, for U.S. Government purposes. Los Alamos National Laboratory requests that the publisher identify this article as work performed under the auspices of the U.S. Department of Energy. Los Alamos National Laboratory strongly supports academic freedom and a researcher's right to publish; as an institution, however, the Laboratory does not endorse the viewpoint of a publication or guarantee its technical correctness.

Form 836 (8/00)

Analytical Solution on the Transient Corrosion/Precipitation in Non-Isothermal Liquid Lead Bismuth Eutectic Flow Loops

J. Zhang‡, and N. Li**

ABSTRACT

Steel corrosion by liquid lead bismuth eutectic (LBE) is one of the critical problems when using the liquid-metal alloy as a coolant in advanced nuclear systems. In a non-isothermal LBE flow loop, the materials corrosion occurs at the hot legs of the circuit and precipitation occurs at some other cooler legs due to mass transfer. In the present study, the transient corrosion and precipitation phenomena in such systems were investigated. An analytical solution was obtained through solving the mass-transfer equation in the boundary layer for the diffusion-limited corrosion process. The temperature-dependent wall corrosion product concentration was a function of the stream-wise coordinate. Solutions for different wall concentration profiles were used to examine the transient process. The initial and final behaviors of the corrosion/precipitation profile are shown for different loop flows. These results reveal important differences between the initial and steady-state corrosion/precipitation phenomena, and how quickly they evolve. This new understanding will help improve the interpretation of the experimental data and the rational application of the corrosion test data to experimental and industrial systems.

KEY WORDS: corrosion rate, flow-induced corrosion, lead-bismuth eutectic, liquid-metal corrosion, mass transfer

INTRODUCTION

Lead bismuth eutectic (LBE) has been a primary candidate material for nuclear coolant and high-power spallation target in accelerator-driven systems (ADS) because of its thermal-physical and chemical properties, such as a low melting point, high thermal conductivity, low vapor pressure, and lack of violent reaction with air and water.[1] However, it is well known that steels are severely corroded by LBE if they are exposed to LBE directly. Corrosion of containment and structural materials presents a critical challenge in the use of LBE as a nuclear coolant in ADS and advanced nuclear reactors.[2] Knowledge of the characteristics of the flow-induced and/or enhanced corrosion is becoming more and more significant in the design and operation of LBE heat-transfer circuits.

Corrosion in LBE systems is primarily due to the relatively high solubility of the base and major alloying components of steels, such as Fe, Ni, Cr, etc., in liquid lead bismuth. The process depends on many factors including the flow velocity, the temperature and thermal gradient, and the compositions of the liquid and solid materials.[3] Without some protective means, the selective dissolution of materials would destroy the containment structure rapidly. Efforts have been devoted to find ways to keep the protective films on the structure to reduce the corrosion rate. It was reportedly achieved in Russia[4] through the application of an active oxygen control technique. By care-

Submitted for publication April 2003; in revised form, August 2003.
‡ Corresponding author. E-mail: jzhang@cnls.lanl.gov.
* Center for Nonlinear Studies, CNLS, MS-B258, Los Alamos National Laboratory, Los Alamos, NM 87545.

0010-9312/04/000043/$5.00+$0.50/0
© 2004, NACE International

fully controlling the oxygen concentration in LBE, it is possible to maintain an iron and chrome oxide-based layer on the surface of structure steels, while keeping lead and bismuth from contamination by excessive oxidization. The oxide film effectively separates the materials from LBE and then the corrosion rate is significantly reduced. The active control allows the maintenance and restoration of the protective oxide films.

For experimental investigation of the corrosion rates in LBE systems, a large number of closed loop systems have been set up to study the flow-induced and/or enhanced corrosion and its mechanism. They are relatively simple and convenient, and representative geometry can be tested in a constant environment for a fixed period.[5] Experiments have been carried out with or without oxygen control to study the corrosion behaviors in LBE flow loops.[6-9] These experiments, however, do not provide a quantitative correlation of the corrosion rate to the hydraulic parameters and the thermal gradient of the loop. In contrast, many corrosion test experiments have been performed in aqueous media.[10-12] Various correlations[13] on corrosion rates for aqueous media have been developed based on the experimental results and phenomenological models. These correlations were used in a previous experiment[13] to calculate the corrosion rate in a liquid-metal environment, and the calculated values were much larger than the experiment results. The test data for corrosion in LBE flow loops remain scattered and difficult to use in more generic systems.

The corrosion product concentrations at the pipe surface are functions of temperature in LBE flow loops with or without the oxygen control. It is the thermal gradient that sustains the corrosion process in a non-isothermal flow loop. Materials are corroded at the hot leg transported to some other cooler legs by the flowing LBE and deposited there.[14] The precipitation of corrosion product at cooler areas of a flow loop may lead to severe flow restrictions, resulting in more deposition there. Except for the importance of precipitation in a non-isothermal LBE flow loop, measured deposition rates in LBE systems are essentially nonexistent as compared to the corrosion rates. Most test loops generally are not designed to investigate deposition characteristics. The deposition of the corrosion product plays important roles in the entire corrosion/precipitation process. Therefore, the precipitation behaviors have to be fully understood at the design stage of practical LBE coolant systems.

Precise simulation of all thermal and hydrodynamic conditions encountered in practical systems by laboratory test systems is difficult and expensive, if not entirely impossible. If the design and operation of an application system do not properly account for corrosion based on limited test data, unforeseen heavy corrosion and precipitation could occur, leading to safety problems.[15] Therefore, it is essential to develop an integral model to interpret and apply the experimental results. In a LBE development program, test loops are made of the same class as the test materials. The up- and downstream effects have to be considered when analyzing/applying the experimental results. Kinetic models have been developed for liquid lead flow loops[16] and liquid lead bismuth flow loops.[17] Both studies indicate that the corrosion/precipitation profile in a non-isothermal liquid-metal loop depends strongly on the axial temperature profile.

Mass transfer plays an important role in flow-induced corrosion, determining the corrosion rate in the mass-transfer-controlled regime.[5] Transients and unsteady states are common and important in many areas of transport applications. There are many industrial applications where knowledge of transient behavior is essential for the design of a control system. Soliman and Chambre[18] studied the time-dependent Leveque problem and obtained an analytical solution for the heat flux under a constant wall temperature by using two Laplace transforms. Mahinpey and Ojha[19] experimentally studied the transient mass transfer in a smooth pipe and obtained the variation of the mass-transfer coefficient with time.

In the present study, an analytical approach is provided to investigate the transient corrosion/precipitation phenomena in LBE flow loop systems. The boundary condition of the corrosion product concentration is a function of the stream-wise coordinate. A general solution is obtained by solving the mass-transfer governing equation in the boundary layer. Based on the transient analysis, the transient period of the corrosion in flow loops and the effects of parameter on the transient process can be determined. The nonlocal analysis provides the maximal values and the corresponding locations of the corrosion and precipitation. The evolution toward steady state also illustrates the source and significance of the differences between open pipe flows and closed loop flows. The methodology of system kinetic modeling and the implication that local corrosion and precipitation can be influenced heavily by system conditions are important for the field of corrosion study.

THEORY

In general, to study the flow-related corrosion, the following mass-transfer equation is considered:

$$\frac{\partial c}{\partial t} + (\vec{u} \cdot \nabla)c = D(\nabla^2 c) \qquad (1)$$

where c (ppm) is the corrosion product concentration, $\vec{u}$ (m/s) is the velocity vector of the flow field, D (m^2/s) is the mass diffusion coefficient, and t (s) is time. Conventionally, the mass-transfer process is

described by dimensionless hydrodynamic and material parameters, such as the Reynolds number (Re) and the Schmidt number (Sc).

The Reynolds number, which determines the flow field characteristics, is defined as:

$$Re = \frac{Ud}{\nu} \tag{2}$$

where U (m/s) is the reference velocity, usually the bulk velocity for fully developed turbulent flow, d (m) is the hydraulic diameter, and ν (m^2/s) is the kinematic viscosity of the fluid.

The Schmidt number, which determines the relationship between the thickness of the hydraulic laminar sub-layer and the thickness of the mass-diffusion boundary layer, is defined as:

$$Sc = \frac{\nu}{D} \tag{3}$$

The higher the Schmidt number is, the thinner the mass-transfer boundary layer will be. For sufficiently high Schmidt numbers, the mass-transfer boundary is submerged under the hydraulic laminar sublayer.

In the present study, a high Schmidt number case was considered that corresponded to liquid-metal media, and the flow was assumed to be fully developed turbulent flow. Therefore, the variation of the corrosion product concentration in any cross section was confined in the thin layer near the wall.[20] Within the mass-diffusion boundary layer, the stream-wise velocity, u, is linearly related to the transverse coordinate, y ($u = \gamma y$, where γ is the wall shear stress rate, $\gamma = \lambda U^2/2\nu$, and λ is the fanning friction factor). From the continuity equation, one readily sees that the transverse velocity is zero. It was assumed that the fluid properties did not change along the loop. With these considerations, the governing mass-transfer equation in the mass-diffusion layer can be simplified:

$$\frac{\partial c}{\partial t} + \gamma y \frac{\partial c}{\partial x} = D\left(\frac{\partial^2 c}{\partial y^2} + \frac{\partial^2 c}{\partial x^2}\right) \tag{4}$$

Introducing the following dimensionless variables:

$$\xi = \frac{x}{L},\ \eta = \left(\frac{\gamma}{DL}\right)^{1/3} y, \tau = \left(\frac{L^2}{\gamma^2 D}\right)^{-1/3} t \tag{5}$$

where L (m) is the loop length. Equation (4) is reduced to:

$$\frac{\partial c}{\partial \tau} + \eta \frac{\partial c}{\partial \xi} = \frac{\partial^2 c}{\partial \eta^2} + p \frac{\partial^2 c}{\partial \xi^2} \tag{6}$$

where:

$$p = \left(\frac{D}{\gamma L^2}\right)^{2/3} \tag{7}$$

The initial condition is $c = 0$ for $\tau = 0$ and $\eta = 0$.

The boundary conditions in a flow-induced corrosion problem depend on the flow velocity. At low velocities, the corrosion rate is completely or partially mass-transfer-controlled. In such a case, the corrosion product concentration at the wall surface (boundary condition) is at its solubility limit or equilibrium state. At high velocities, the dissolution reactions (without oxygen control) or reduction reactions (with oxygen control) at the solid-liquid interface become the limiting step, and the corrosion rate is determined by the reaction rate. Most of the studies performed in liquid metal have shown that a corrosion process is controlled by mass transfer.[13] Therefore, it is reasonable to assume that the corrosion product concentration at the solid-liquid interface equals its solubility or equilibrium concentration and does not vary with time in the LBE flow loop. For the dissolution process, the surface concentrations are equal to their saturated concentrations:[21]

$$\log(c) = \log(c_s) = A_1 + \frac{B_1}{T} \tag{8}$$

where T is the absolute temperature in Kelvin and c_s is the solubility concentration in ppm. The values of parameters A_1 and B_1 vary among species, and some of them for common components in steels and oxygen can be found elsewhere.[21] In the reduction process, the protective MO_β-based film can be reduced by Pb and the equilibrium concentration of M is:

$$\log(c_{eq}) = A_2 - \frac{B_2}{T} - \beta \log(c_o) \tag{9}$$

where c_O is the oxygen concentration in LBE; c_{eq} is the equilibrium concentration of species M; A_2 and B_2 vary for species and can be calculated through analyzing the oxygen thermodynamic activity in LBE,[21] for example, for iron (main corrosion product), $A_2 = 11.35$, $B_2 = 12{,}844$, and $\beta = 4/3$.

There is a critical oxygen level in LBE, below which no continuous iron oxide-based film can exist and the Fe concentration at the surface is given by Equation (8). Above that oxygen level, a continuous iron oxide film can form and the Fe concentration is given by Equation (9). It is not clear how these two regions connect to each other. He, et al.,[22] assumes that the species concentration at surfaces is given by the minimum of the saturation concentration and the chemical equilibrium concentration. That is:

$$c_w = \min(c_s, c_{eq}) \quad (10)$$

Therefore, the corrosion product concentration (mainly iron) at the pipe surface is a function of temperature in LBE flow loops with or without the oxygen control. In a non-isothermal flow loop, it is a function of the stream-wise coordinate and the boundary conditions for Equation (6) can be written as follows:

$$\begin{aligned} &c = c_w(\xi) \text{ for all } \tau \text{ and } \eta = 0, \\ &\text{and } c \text{ is finite for all } \tau \text{ and } \eta \to \infty. \end{aligned} \quad (11)$$

Considering a closed loop flow, the surface concentration can be expressed as a periodic function. Hence, it can be written in the following Fourier series:

$$c\,|_{\eta=0} = c_w(\xi) = \sum_k a_k e^{2k\pi i\xi} (0 \le \xi \le 1) \quad (12)$$

ANALYTICAL SOLUTION

To solve the present problem, the concentration is expanded in a Fourier series:

$$c(\tau, \eta, \xi) = \sum_k Y_k(\tau, \eta) e^{2k\pi i\xi} \quad (13)$$

Each $Y_k(\tau,\eta)$ satisfies the following ordinary differential equation (ODE):

$$\begin{aligned} &\frac{\partial Y_k(\tau,\eta)}{\partial \tau} + 2ik\pi\eta Y_k(\tau,\eta) = \\ &\frac{\partial^2 Y_k(\tau,\eta)}{\partial \eta^2} - 4\pi^2 k^2 p Y_k(\tau,\eta) \end{aligned} \quad (14)$$

The initial condition and boundary condition are $Y_k(0,\eta > 0) = 0$, $Y_k(\tau,\eta = 0) = a_k$ and $Y_k(\tau,\eta \to \infty)$ is finite.

Applying the Laplace transform with respect to the variable τ:

$$L\left[Y_k(\tau,\eta)\right] = \tilde{Y}_k(s,\eta) \quad (15)$$

we obtain:

$$\begin{aligned} &s\tilde{Y}_k(s,\eta) + 2ik\pi\eta\tilde{Y}_k(s,\eta) = \\ &\frac{\partial^2 \tilde{Y}_k(s,\eta)}{\partial \eta^2} - 4\pi^2 k^2 p \tilde{Y}_k(s,\eta) \end{aligned} \quad (16)$$

with boundary conditions $\tilde{Y}_k(s,0) = a_k/s$ and $\tilde{Y}_k(s,\eta \to \infty)$ is finite. We then obtain:

$$\tilde{Y}_0(s,\eta) = \frac{a_0}{s} \exp(-\sqrt{s}\eta) \quad (17)$$

and:

$$\begin{aligned} \tilde{Y}_k(s,\eta) = &\frac{a_k}{sAi[(2ik\pi)^{-2/3}(s + 4\pi^2k^2p)]} \times \\ &Ai[(2ik\pi)^{-2/3}(s + 4\pi^2k^2p + 2ik\pi\eta)] \end{aligned} \quad (18)$$

where Ai is the Airy Function:

$$\begin{aligned} Ai(x) = &3^{-2/3} \sum_{n=0}^{\infty} \frac{1}{n!} \sin[2/3(n+1)\pi] \\ &\int_0^{\infty} z^{n/3-2/3} e^{-z} dz (3^{1/3}x)^n \end{aligned} \quad (19)$$

The inverse Laplace transformation for k = 0 is:

$$Y_0(\tau,\eta) = a_0 - a_0 Erf\left(\frac{\eta}{2\sqrt{\tau}}\right) \quad (20)$$

where Erf is the Error Function:

$$Erf(x) = \frac{2}{\sqrt{\pi}} \int_0^x e^{-z^2} dz \quad (21)$$

For k > 0, according to the invert method given elsewhere,[18] for $\eta << 1$, we get:

$$\begin{aligned} Y_k(\tau,\eta) = &\frac{a_k Ai[(2ik\pi)^{-2/3}(4\pi^2k^2p + 2ik\pi\eta)]}{Ai[(2ik\pi)^{-2/3}4\pi^2k^2p]} \\ &+ a_k \sum_{n>0} \frac{Ai[(2ik\pi)^{-2/3}(s_n + 4\pi^2k^2p + 2ik\pi\eta)]}{s_n(2ik\pi)^{-2/3}Ai'[(2ik\pi)^{-2/3}(s_n + 4\pi^2k^2p)]} \exp(s_n\tau) \end{aligned} \quad (22)$$

where $s_n = -(2\pi ki)^{2/3}c_n - 4\pi^2k^2p$ and $-c_n$ are the zeros of the Airy Function.[23] For k < 0, since the concentration is real:

$$Y_{k<0}(\tau,\eta) = \overline{Y}_{|k|}(\tau,\eta) \quad (23)$$

the bar represents the conjugate term. Taking into account that Ai(x) oscillates with x when Real(x) < 0 and the boundary condition that the concentration is finite when $\eta \to \infty$, it requires $i^{1/3} = \sqrt{3}/2 + i/2$ and $i^{2/3} = 1/2 + \sqrt{3}i/2$.

The mass flux (corrosion or precipitation) in the transform domain is defined by:

$$\begin{aligned} q = -D\frac{\partial c}{\partial y}\,|_{y=0} = -&\left(\frac{\gamma D^2}{L}\right)^{1/3} \times \\ &\left\{\frac{\partial Y_0}{\partial \eta} + \sum_{k\neq 0} \frac{\partial Y_k}{\partial \eta} \exp(2ik\xi\pi)\right\}|_{\eta=0} \end{aligned} \quad (24)$$

where:

$$\frac{\partial Y_0}{\partial \eta}\Big|_{\eta=0} = -\frac{a_0}{(\pi\tau)^{1/2}} \tag{25}$$

and:

$$\frac{\partial Y_{k>0}(\tau,\eta)}{\partial \eta}\Big|_{\eta=0} = (2ik\pi)^{1/3}\frac{a_k Ai'[(2ik\pi)^{-2/3}4\pi^2k^2p]}{Ai[(2ik\pi)^{-2/3}4\pi^2k^2p]} + (2ik\pi)^{1/3}a_k\sum_{n>0}\frac{1}{s_n(2ik\pi)^{-2/3}}\exp(s_n\tau) \tag{26}$$

$$\frac{\partial Y_{k<0}(\tau,\eta)}{\partial \eta}\Big|_{\eta=0} = \frac{\partial \overline{Y}_{|k|}(\tau,\eta)}{\partial \eta}\Big|_{\eta=0} \tag{27}$$

The steady state solution is:

$$c_{ss} = \lim_{\tau\to\infty} c = \sum_k \Phi_k \exp(2k\pi i\xi) \tag{28}$$

$$q_{ss} = \lim_{\tau\to\infty} q = -\left(\frac{\gamma D^2}{L}\right)^{1/3}\sum_k \Psi_k \exp(2k\pi i\xi) \tag{29}$$

where:

$$\Phi_0 = a_0, \Phi_{k<0} = \overline{\Phi}_{|k|}, \Phi_{k>0} = \frac{a_k Ai[(2ik\pi)^{-2/3}(4\pi^2k^2p + 2ik\pi\eta)]}{Ai[(2ik\pi)^{-2/3}4\pi^2k^2p]} \tag{30}$$

and:

$$\Psi_0 = 0, \Psi_{k<0} = \overline{\Psi}_{|k|}, \Psi_{k>0} = (2ik\pi)^{1/3}\frac{a_k Ai'[(2ik\pi)^{-2/3}4\pi^2k^2p]}{Ai[(2ik\pi)^{-2/3}4\pi^2k^2p]} \tag{31}$$

Thus, the analytical solution is completed for the transient and steady state of the corrosion product concentration and the corrosion/precipitation rate for a turbulent closed loop flow. It should be pointed out that the solution of the corrosion product concentration is only valid near the pipe surface. When $q > 0$, the corrosion product flux is from the pipe wall to the fluid, corresponding to corrosion. When $q < 0$, the mass flux is from the bulk fluid to the wall, corresponding to precipitation. For highly turbulent flow, the axial diffusion term is negligible ($p \to 0$, see Discussion). We then get the solution that is identical to the steady-state solution obtained elsewhere[17] in which the axial diffusion term is neglected.

The present solution was obtained based on the assumption that the stream-wise velocity, u, is linearly related to the transverse coordinate near the vessel wall. For the fully developed laminar flow, the assumption is still reasonable under Leveque assumption.[24]

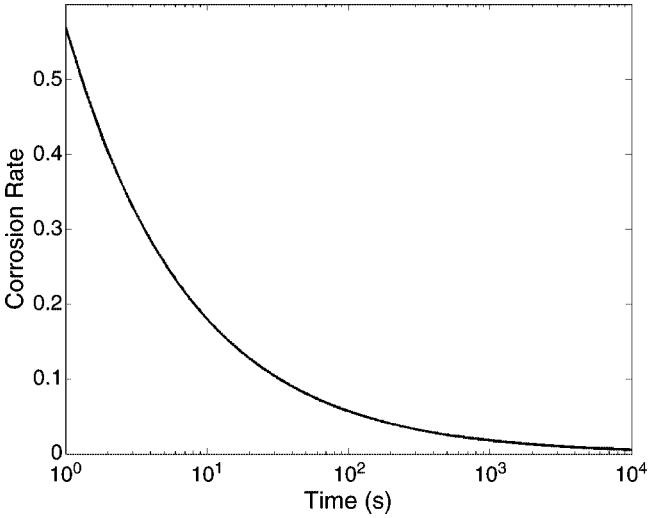

FIGURE 1. *Corrosion rate for an isothermal loop flow vs time. The corrosion rate is scaled as $q/\tilde{c}\sqrt{D}$.*

ANALYSIS RESULTS

Loop with Constant Wall Surface Concentration

This case corresponds to an isothermal loop flow. Under the constant temperature, the wall corrosion product concentration stays constant along the loop axis, i.e., $c_w = \tilde{c}$, where $\tilde{c}$ is constant. The corrosion product concentration and the corrosion rate for this case are:

$$\frac{c}{\tilde{c}} = 1 - \mathrm{Erf}\left(\frac{\eta}{2\sqrt{\tau}}\right) = 1 - \mathrm{Erf}\left(\frac{y}{2\sqrt{Dt}}\right) \tag{32}$$

$$\frac{q}{\tilde{c}} = \left(\frac{\gamma D^2}{L}\right)^{1/3}\frac{1}{(\pi\tau)^{1/2}} = \sqrt{\frac{D}{\pi t}} \tag{33}$$

Equations (32) and (33) indicate that the concentration profile and the corrosion rate for isothermal loop flow are independent of the hydraulic factors, such as the flow velocity, the hydraulic diameter, and the loop length. The solution is similar to 1-D diffusion problems. When $t \to \infty$, the concentration approaches a uniform distribution, $c = \tilde{c}$, and the mass flux of the corrosion product stops because there is no concentration gradient between wall and the bulk fluid. For an isothermal loop flow, although corrosion may proceed initially if there is a concentration difference between the wall surface and the bulk fluid, it will eventually stop once the solution becomes saturated with the corrosion product (Figure 1).

Loop with Sinusoidal Concentration Profile

To determine the corrosion/precipitation profile in a non-isothermal flow loop, the surface concentration must be specified. One of the simplest functional forms is the sinusoidal concentration profile. Suppose that the surface concentration has the following distribution:

$$c_w = \tilde{c}[1 + \sigma \cos(2\pi x / L)] \quad (34)$$

where $\tilde{c}$ is constant and 2σ is the concentration oscillation. For this idealized surface concentration profile, the concentration distribution is:

$$\frac{c}{\tilde{c}} = 1 - \mathrm{Erf}\left(\frac{\eta}{2\sqrt{\tau}}\right) + Y_1 \exp(2\pi i\xi) + \overline{Y}_1 \exp(-2\pi i\xi) \quad (35)$$

where:

$$Y_1(\tau,\eta) = \frac{1}{2}\sigma\left[\frac{\mathrm{Ai}[(2i\pi)^{-2/3}(4\pi^2 p + 2i\pi\eta)]}{\mathrm{Ai}[(2i\pi)^{-2/3}4\pi^2 p]} + \sum_{n>0} \frac{\mathrm{Ai}[(2i\pi)^{-2/3}(s_n + 4\pi^2 p + 2i\pi\eta)]}{s_n (2i\pi)^{-2/3}\mathrm{Ai}'[(2i\pi)^{-2/3}(s_n + 4\pi^2 p)]} \exp(s_n\tau)\right] \quad (36)$$

and the corrosion rate can be written as:

$$\frac{q}{\tilde{c}} = -\left(\frac{\gamma D^2}{L}\right)^{1/3}\left[-\frac{1}{(\pi\tau)^{1/2}} + \frac{\partial Y_1}{\partial\eta}\Big|_{\eta=0} \exp(2i\xi\pi) + \frac{\partial \overline{Y}_1}{\partial\eta}\Big|_{\eta=0} \exp(-2i\xi\pi)\right] \quad (37)$$

where:

$$\frac{\partial Y_1(\tau,\eta)}{\partial\eta}\Big|_{\eta=0} = \frac{1}{2}\sigma\left[(2i\pi)^{1/3}\frac{\mathrm{Ai}'[(2i\pi)^{-2/3}4\pi^2 p]}{\mathrm{Ai}[(2i\pi)^{-2/3}4\pi^2 p]} + 2i\pi\sum_{n>0}\frac{1}{s_n}\exp(s_n\tau)\right] \quad (38)$$

The corrosion/precipitation rate profile developing with time along the loop is shown in Figure 2. There are several notable features. At early times, there is no precipitation anywhere in the flow loop. The highest/lowest corrosion occurs at the place where the surface concentration is maximal/minimal. As time increases, the highest/lowest corrosion rate decreases and their locations moves in the opposite direction of the stream-wise flow. Precipitation first occurs at the position before the location of the minimal surface concentration and spreads upstream until the process reaches the steady state. At the steady state, the highest corrosion/precipitation rate does not occur at the highest/lowest surface concentration. Instead, there is a phase shift between the location of the highest corrosion/precipitation and that of the highest/lowest surface concentration. The phase decreases while the nondimensional highest corrosion/precipitation rate increases as the axial diffusion effect increases.

For the high Reynolds numbers, the parameter, p, approaches zero and the axial diffusion term in the mass-transfer equation (Equation [6]) can be neglected (see Discussion). Then, from Equation (37), for the sinusoidal surface concentration profile we obtain:

$$\lim_{p\to 0} q_{ss} = -\left(\frac{\gamma D^2}{L}\right)^{1/3}\sigma\tilde{c}(2\pi)^{1/3}\times \frac{\mathrm{Ai}'[0]}{\mathrm{Ai}[0]}\cos[2(\pi\xi + \pi/12)] \quad (39)$$

where $\mathrm{Ai}'(0) = -0.2588$ and $\mathrm{Ai}(0) = 0.3550$. It indicates the phase shift between the location of the highest corrosion/precipitation, and that of the highest/lowest surface concentration approaches one-twelfth of the loop length with the Reynolds number increasing. Although this phase shift value is not generally applicable for all surface concentration profiles, it shows that the corrosion/precipitation rate profile depends only on the surface concentration profile for high Reynolds numbers at steady state. Increasing the Reynolds number only results in higher corrosion and higher precipitation, while the shape of the corrosion/precipitation distribution does not change.

For closed loop flow systems, the total amount of corrosion equals the total amount of precipitation at steady state because the fluid cannot be replenished; that is, the average corrosion rate is zero at the steady state. Figure 3 shows the change of the average corrosion rate with time. The average corrosion rate decreases rapidly at the beginning and gradually vanishes as the dimensionless time increases. This function is independent of the axial diffusion term. Judging from the definition of the dimensionless time, increasing the flow velocity reduces the actual transient time, while increasing the loop length increases it.

Materials Test Loop

The materials test loop (MTL) is a non-isothermal closed loop and is used to study the corrosion of various materials in flowing LBE in the Los Alamos National Laboratory (LANL). It uses a recuperator, a heater, and a heat exchanger to set and control the temperature profile. LBE comes out of the pump at a low temperature, passes through the recuperator shell side and the heater, and reaches the highest

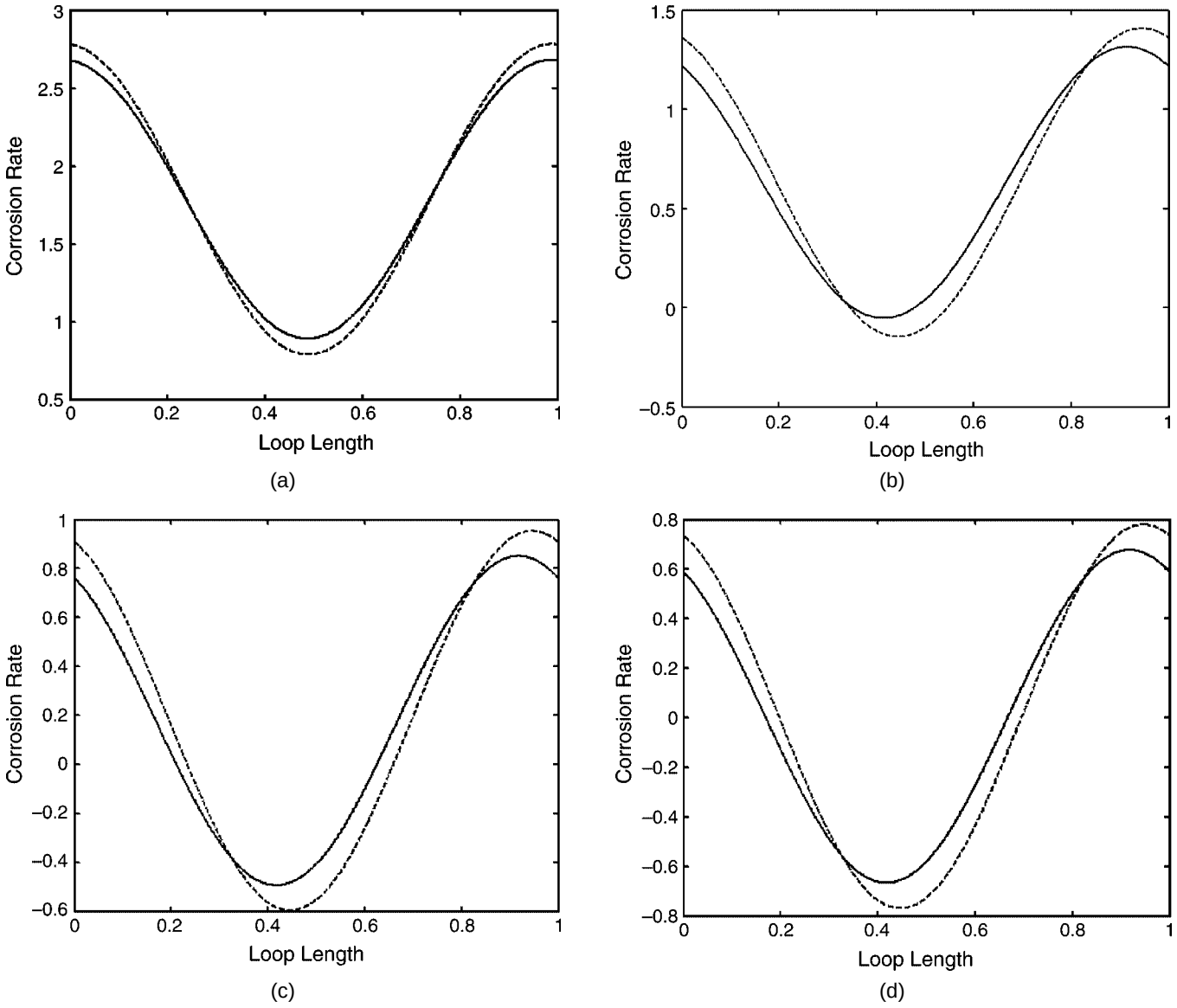

FIGURE 2. *Transient corrosion/precipitation rate distribution for sinusoidal surface concentration for different dimensionless time. The rate is scaled as* $q(\gamma D^2/L)^{-1/3}/\tilde{c}$. $\sigma = 0.5$, *dashed line* $p = 0.03$, *and solid line* $p = 10^{-4}$. *(a)* $\tau = 0.1$; *(b)* $\tau = 0.8$; *(c)* $\tau = 10$; *(d)* $\tau = 10^5$.

temperature at the test section. On the return path, the temperature decreases through the recuperator tube side and the heat exchanger, and reaches the lowest temperature. A temperature profile is shown in Figure 4.

In the oxygen-controlled MTL loop, it is assumed that the protective oxide-layer (Fe_3O_4) is formed and the oxygen concentration in LBE is controlled to be a constant value through the oxygen control facility. Equation (10) is used to calculate the iron surface concentration.

The loop length, L, is 30.0 m and the vessel inner diameter, d, is 0.0525 m. The LBE flow velocity, U, is 0.5 m/s. The kinematic viscosity (ν) of the LBE and the diffusion coefficient of iron into LBE (D) are functions of the temperature. In the present model, it is assumed to be a constant and we estimate $\nu = 1.5 \times 10^{-7}$ m^2/s and $D = 10^{-9}$ m^2/s.[22] The following was obtained: $\gamma = 3427.4$ s^{-1}, $p = 4.7 \times 10^{-11}$, where the Blasius Equation[19] is used to calculate the friction factor λ($\lambda = 0.046 Re^{-0.20}$).

The transient corrosion/precipitation rates for the loop at different times from the present model are shown in Figure 5. At the beginning, corrosion (positive value of the flux) occurs everywhere in the loop. As time goes by, the corrosion rate in the maximal temperature section decreases. Precipitation (negative value of the flux) does not appear first at the lowest temperature section. Instead, it occurs at a location shortly downstream from the maximal tem-

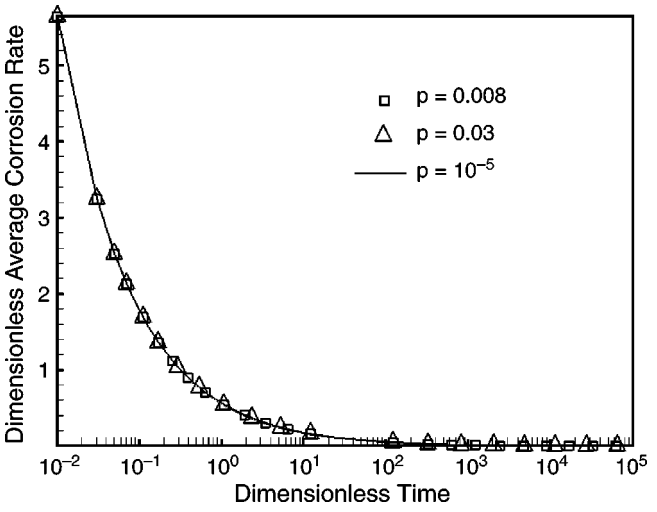

FIGURE 3. *Dimensionless average corrosion rate for a sinusoidal surface concentration with the dimensionless time. The rate is scaling as* $q(\gamma D^2/L)^{-1/3}/\tilde{c}$.

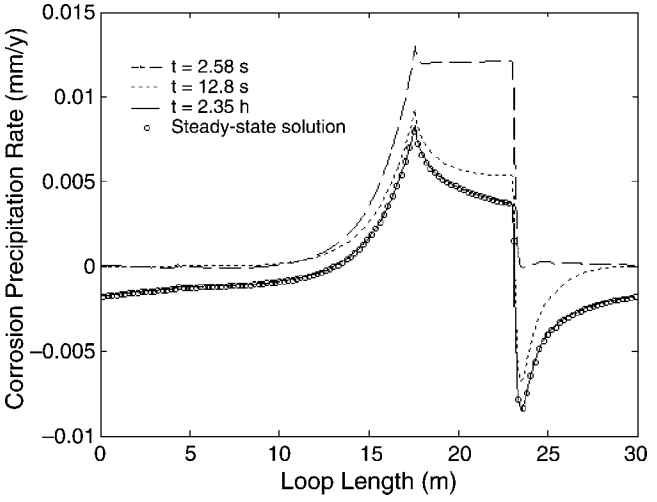

FIGURE 5. *Transient Fe corrosion/precipitation rate distribution for MTL.* T_{Int} *= 450°C,* T_{Max} *= 550°C,* T_{Min} *= 350°C,* c_o *= 0.01 ppm.*

perature section. The distribution quickly evolves toward the steady state. At the steady state, the highest corrosion occurs at the end of the heater zone where the temperature first reaches the maximum. The corrosion rate then steadily decreases in the maximal temperature section, clearly demonstrating the "downstream" effects from some earlier corrosion tests. The highest precipitation occurs at the return side of the recuperator where the temperature is in the intermediate range, rather than at the end of the heat exchanger where the temperature is at the lowest. This shows that the corrosion/precipitation distribution depends strongly on the global temperature distribution.

The corrosion/precipitation distribution in the test loop can be best understood from the concentration distribution near the pipe walls. Figure 6 shows the development of Fe concentration distribution in the near-wall region with time. Initially, the Fe concentration in the bulk fluid is zero, and there is a negative concentration gradient between the bulk fluid and the interface at the vessel wall. Therefore, corrosion occurs everywhere in the loop. As time goes by, the corrosion product diffuses into the bulk fluid and the Fe concentration in the bulk fluid increases and reaches the steady-state value. The average value of the bulk concentration equals the average of the pipe surface concentration (for the present case, it is 0.00675 ppm). The thickness of the mass-transfer boundary layer where the concentration changes sharply is about 0.25 mm. In the bulk fluid, the Fe concentration is quite uniform.

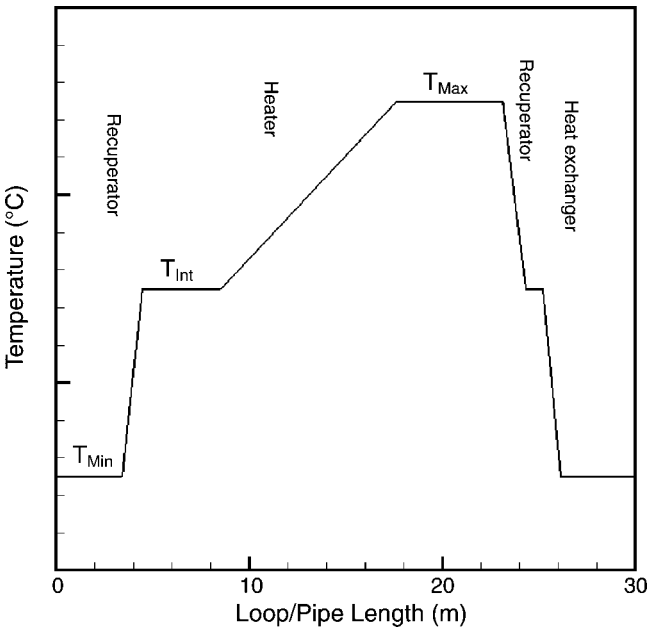

FIGURE 4. *Temperature profile of the LBE test loop (MTL).* T_{Max}*: maximal temperature;* T_{Min}*: minimal temperature;* T_{Int}*: intermediate temperature.*

The variation of the transient average corrosion rate in the highest temperature section for different temperature gradients between the highest and the lowest temperatures is shown in Figure 7. The transient corrosion rate decreases rapidly at the early times, slows after about 10 s, and nearly reaches the steady-state value after about 200 s. This time is short enough to be neglected in long-term applications for the LBE system. The temperature gradient has little effect on the transient time, while it significantly affects the steady-state corrosion rate. The corrosion rate increases with increasing temperature gradient. Again, this demonstrates that the corrosion rate at a constant temperature section in a non-isothermal system depends on both the local and global conditions.

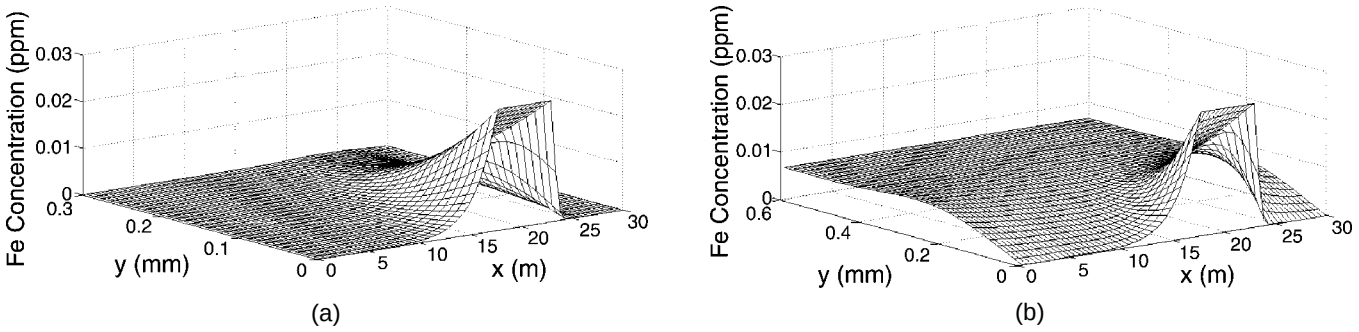

FIGURE 6. *Transient Fe concentration profile for MTL. T_{Int} = 450°C, T_{Max} = 550°C, T_{Min} = 350°C, c_o = 0.01 ppm. (a) t = 8.9 s and (b) t = 119 h.*

In an oxygen-controlled LBE system, the surface Fe concentration is a function of the oxygen concentration in LBE. The corrosion can proceed via dissolution at very low oxygen concentrations, and through surface oxidation and reduction of surface oxides at higher oxygen concentrations. The effects of oxygen concentration on the transient corrosion rate are shown in Figure 8. The corrosion rate decreases as the oxygen concentration in LBE is increased. The transient profile of the average corrosion rate changes little with the oxygen concentration.

DISCUSSION

A general solution for the transient corrosion process in loop systems has been obtained under the assumptions that the stream-wise velocity is linearly related to the transverse coordinate in the concentration boundary layer, and that there is no internal source or sink of corrosion product. The solution takes into account both the transverse and axial diffusion terms. However, by analyzing the solution for a test loop, the axial diffusion term (the second term on the right-hand side of Equation [6]) was found to be small enough to be neglected. The coefficient of the axial diffusion term, p, can be rewritten as:

$$p = \left(\frac{D}{\gamma L^2}\right)^{2/3} = 12.4\,Re^{-1.2}\,Sc^{-0.67}(d/L)^{4/3} \qquad (40)$$

For the present solution, the Schmidt number Sc >> 1, and in most engineering applications, the flow is highly turbulent, Re >> 1, and the hydraulic diameter, d, is much smaller than the loop length, L (i.e., d/L << 1). Therefore, p << 1 and the axial diffusion term can be neglected. The corrosion flux is reduced to:

$$q = 0.2844\,Re^{0.6}\,Sc^{1/3}\left(\frac{d}{L}\right)^{1/3}\frac{D}{d}\left[\frac{a_0}{(\pi\tau)^{1/2}} - \sum_k \Psi_k(p=0)\exp(2\pi k i\xi) + \sum_k H_k(\tau)\exp(2\pi k i\xi)\right] \qquad (41)$$

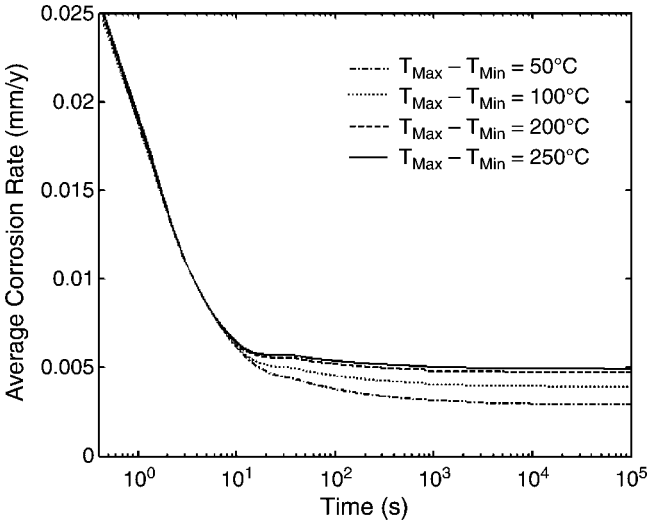

FIGURE 7. *Temporal evolution of the transient average corrosion rate for MTL in the highest temperature section for different temperature gradients. c_o = 0.01 ppm, T_{Max} = 550°C.*

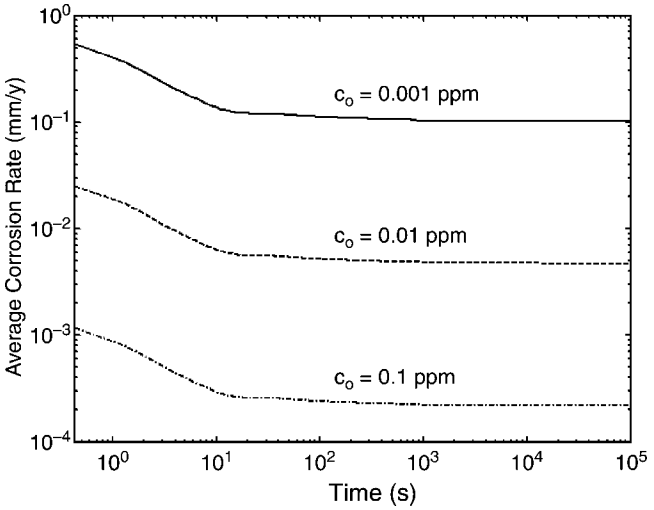

FIGURE 8. *Temporal evolution of the transient average corrosion rate for MTL at the highest temperature section for different oxygen concentration in LBE. T_{Int} = 450°C, T_{Max} = 550°C, T_{Min} = 350°C.*

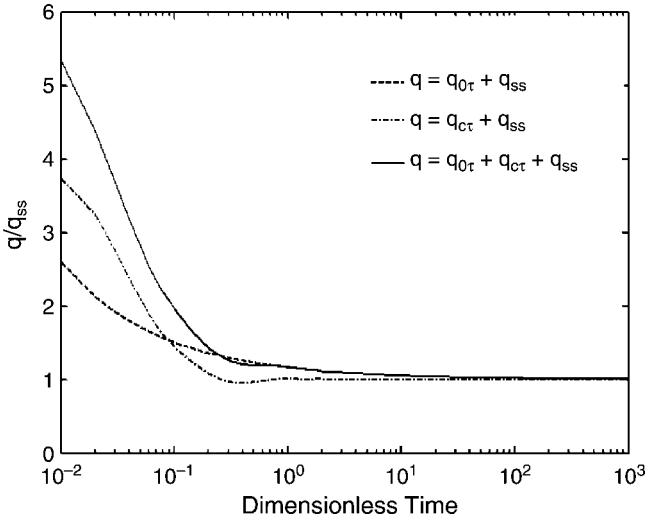

FIGURE 9. *Relative contribution to the average transient corrosion rate for MTL at the test section. T_{Int} = 450°C, T_{Max} = 550°C, T_{Min} = 350°C, c_o = 0.01 ppm.*

where:

$$\Psi_0(p=0)=0,\ \Psi_{k>0}(p=0)=(2\pi ki)^{1/3}a_k\ \frac{Ai'(0)}{Ai(0)},\ \Psi_{k<0}(p=0)=\overline{\Psi}_{|k|}(p=0) \quad (42)$$

and:

$$H_0(\tau)=0,\ H_{k>0}(\tau)=(2\pi ki)^{1/3}a_k\sum_{n>0}\frac{1}{c_n}\exp[-(2k\pi i)^{2/3}c_n\tau],\ H_{k<0}(\tau)=\overline{H}_{|k|}(\tau) \quad (43)$$

Equation (41) indicates that the kinetic corrosion/precipitation rate in a non-isothermal closed loop flow system scales as $Sc^{1/3}$ and is the same as in open pipe flow with high Schmidt numbers. The dependence on the Reynolds number is $Re^{0.6}$ and is smaller than that of a pipe flow.[13] Increasing the flow velocity results in higher local corrosion/precipitation rates, while increasing the loop length reduces the local corrosion/precipitation rate.

If the corrosion/precipitation rate scales $a_0Re^{0.6}Sc^{1/3}\ (d/L)^{1/3}\ D/d$, Equation (41) shows that the nondimensional corrosion/precipitation rate is independent of the hydraulic factors for high Reynolds numbers. For a specified dimensionless time, τ, the corrosion/precipitation profile is determined only by the surface temperature profile or the resultant corrosion product concentration profile.

Equation (41) indicates that the transient corrosion/precipitation rate consists of three terms—the transient term related to the average surface concentration:

$$q_{0\tau}=\left(\frac{\gamma D^2}{L}\right)^{1/3}\frac{1}{(\pi\tau)^{1/2}}a_0=a_0\sqrt{\frac{D}{\pi t}} \quad (44)$$

the steady-state term only dependent on the surface concentration profile:

$$q_{ss}=-\left(\frac{\gamma D^2}{L}\right)^{1/3}\sum_k\Psi_k(p=0)\exp(2\pi ki\xi) \quad (45)$$

and the transient term related to the surface concentration profile:

$$q_{c\tau}=\left(\frac{\gamma D^2}{L}\right)^{1/3}\sum_k H_k(\tau)\exp(2\pi ki\xi) \quad (46)$$

The first term is independent of the hydraulic parameters and can be seen as the solution of the 1-D diffusion problem. To find out the relative importance of the three terms on the transient process, three curves are shown in Figure 9. It is clear that the term $q_{c\tau}$ tends to zero at large times and it is important at early times. At later times, the transient characteristics are dominated by the $q_{0\tau}$ term, which is independent of the flow velocity. It may be noted that the transient corrosion approaches the steady state after the dimensionless time exceeds one.

The solution of the corrosion product concentration is only valid in the sub-laminar layer; that is, $\eta << 1$. However, using the solution, a constant bulk concentration was predicted that equals the average surface concentration (Figure 6). In fact, the bulk concentration can be obtained through solving the mass-transfer equation in the bulk flow. Neglecting the diffusion terms, Zhang and Li gave a solution of the bulk concentration at steady state as:[25]

$$c_b(\xi)=a_0+\frac{4}{Vd}\frac{(2\pi L^2D^2\gamma)^{1/3}}{3^{1/3}Ai(0)\Gamma(1/3)}\sum_k B_k\exp(2\pi ki\xi) \quad (47)$$

where $B_0 = 0$, $B_{k>0} = \frac{a_k}{2\pi(ki)^{2/3}}$, and $B_{k<0} = \overline{B}_{|k|}$. Equation (47) shows that average bulk concentration is a_0, which is exactly the same as the value obtained from the solution in the sub-laminar layer when $\eta \to \infty$. The bulk concentration varies around the average value along the axis of the loop, but the variation is small enough to be neglected.[25] In a practical LBE loop, it is reasonable to assume the bulk concentration is constant over the entire loop.

The present solution is valid for the cases in which the concentration boundary layer is submerged in the hydraulic boundary layer (i.e., for high Schmidt number situations such as corrosion in flowing liquid-metal systems). This condition will change for other fluids and more sophisticated mod-

els are necessary for analyzing corrosion/precipitation in those systems. When there are chemical reactions between the corrosion product and the media in the bulk fluid, the mass-transport equation must be expanded to include the additional species and reaction kinetics. We will investigate this in the near future.

CONCLUSIONS

❖ In the present study, a kinetic corrosion model was developed to study the transient corrosion/precipitation phenomena in closed flow loops with high Schmidt numbers. The model is based on solving the mass-transfer equation in the mass-transfer boundary layer.

❖ The transient corrosion/precipitation distribution depends on both local and global conditions. Corrosion occurs everywhere in the loop at the beginning and precipitation appears at some locations in later times. At the steady state, the highest corrosion/precipitation does not occur at the location with the highest/lowest temperature (or surface corrosion product concentration), and the corrosion product concentration in the bulk flow is almost uniform, and the average value equals the average value of that of the surface concentration. The axial diffusion contribution can be neglected for high Reynolds numbers, and the corresponding corrosion/precipitation distribution profile is independent of the flow velocity and is determined by the temperature (surface concentration) profile. The transient term related to the global concentration profile plays an important role at the early times, while the transient term related to the mean surface concentration dominates the transient process at later times.

❖ For the materials test loop, the corrosion rate at the maximal temperature section (the primary test section) decreases rapidly in time and reaches the steady-state value after about 200 s. This time is independent of the temperature gradient and the oxygen concentration in LBE. The decrease is more significant further down the stream, calling attention to the need to record the test locations and properly interpret the test results. The corrosion rate increases with the increasing temperature gradient and the decreasing oxygen concentration. This model provides a location-resolved corrosion/precipitation rate that cannot be obtained easily from the conventional local mass-transfer models, and clearly illustrate the source of the differences between open pipe flows and closed loop flows.

ACKNOWLEDGMENTS

This research was supported by the Department of Energy under contract no. W-7405-ENG-36.

REFERENCES

1. P. Deloffre, A. Terlaani, F. Barbier, J. Nucl. Mater. 301 (2002): p. 35.
2. J.J. Park, D.P. Butt, C.A. Beard, Nucl. Eng. Des. 196 (2000): p. 315.
3. G. Ilincev, Nucl. Eng. Des. 217 (2002): p. 167.
4. B.F. Gromov, Y.S. Belomitcev, E.I. Yefimov, M.P. Leonchuk, P.N. Martinov, Y.I. Orlov, D.V. Pankratov, Y.G. Pashkin, G.I. Toshinsky, V.V. Chekunov, B.A. Shmatko, V.S. Stepanov, Nucl. Eng. Des. 173 (1997): p. 207.
5. Z. Ahmed, B.J. Abdul Aleem, J. Mater. Eng. Perform. 3 (1994): p. 393.
6. D.G. Briceno, F.J.M. Munoz, L.S. Crespo, F. Esteban, C. Torres, J. Nucl. Mater. 296 (2001): p. 265.
7. H. Glasbrenner, J. Konys, G. Mueller, A. Rusanov, J. Nucl. Mater. 296 (2001): p. 237.
8. G. Muller, A. Heinzel, J. Konys, G. Schumacher, Weisenburger, F. Zimmermann, V. Engelko, A. Rusanov, V. Markov, J. Nucl. Mater. 301 (2002): p. 40.
9. F. Barbier, A. Rusanov, J. Nucl. Mater. 296 (2001): p. 231.
10. F.P. Berger, K.F.F.L, Hau, Int. J. Heat Mass Trans. 20 (1977): p. 1,185.
11. D.C. Silverman, Corrosion 40 (1984): p. 220.
12. P. Harriott, R.M. Hamilton, Chem. Eng. Sci. 20 (1965): p. 1,073.
13. F. Balbaud-Celerier, F. Barbier, J. Nucl. Mater. 289 (2001): p. 227.
14. P.F. Tortorelli, O.K. Chopra, J. Nucl. Mater. 103, 104 (1981): p. 621.
15. J. Konys, H. Muscher, Z. Voss, O. Wedemeyer, J. Nucl. Mater. 296 (2001): p. 289.
16. J. Sannier, G. Santarini, J. Nucl. Mater. 107 (1982): p. 196.
17. J. Zhang, N. Li, J. Nucl. Mater. 321 (2003): p. 184.
18. M. Soliman, P. Chambre, Int. J. Heat Mass Trans. 10 (1967): p. 169.
19. N. Mahinpey, M. Ojha, O. Trass, Int. J. Heat Mass Trans. 44 (2001): p. 3,919.
20. W.V. Pinczewski, S. Sideman, Chem. Eng. Sci. 29 (1974): p. 1,969.
21. N. Li, J. Nucl. Mater. 300 (2002): p. 73.
22. X. He, N. Li, M. Mineev, J. Nucl. Mater. 297 (2001): p. 214.
23. J.C.P. Milier, The Airy Integral (Cambridge, U.K.: Cambridge University Press, 1946), p. 43.
24. W.M. Leslie, J.A. Alden, R.G. Compton, T. Silk, J. Phys. Chem. 100 (1996): p. 14,130.
25. J. Zhang, N. Li, J. Nucl. Sci. Technol. 3 (2004): in press.